Research Article

Performance Evaluation of Solar Parabolic Collector Using Low Volume Fractions of Multi-Walled Carbon-nanotube in Synthetic Engine Oil

Vinayak Talugeri*, Veeranna Basawannappa Nasi, Gururaj Lalagi and Nagaraj Basavaraj Pattana
Department of Mechanical Engineering, M. S. Ramaiah Institute of Technology, Visvesvaraya Technological University, Belagavi, India

* Corresponding author. E-mail: vinayaktalugeri@gmail.com DOI: 10.14416/j.asep.2024.06.005
Received: 2 February 2024; Revised: 12 March 2024; Accepted: 28 March 2024; Published online: 17 June 2024

Abstract
The use of nanofluids has been encouraged to advance the efficiency of solar collectors in previous investigations. In this experiment, the performance of solar parabolic collectors in Bangalore, India, was enhanced using low-volume fractions of multi-walled carbon nanotubes (MWCNT) and synthetic engine oil as the base fluid. To stabilize and optimize the thermal conductivity of the nanofluids, orthocresol was used as a surfactant and was further treated with magnetic stirring and ultrasonication. The resulting MWCNT-synthetic engine oil nanofluid was generated at three different volume fractions with a 1:1 MWCNT/ Orthocresol ratio and tested at different flow rates between 10:00 and 16:00 according to ASHRAE Standards. The maximum efficiency was achieved at 0.0317 vol% and a discharge of 7 L/min, which was 6.9% higher than that of the synthetic engine oil. This study shows that even at low-volume fractions of nanofluids, effective heat transfer can be achieved in solar parabolic collectors. These findings suggest that MWCNT-synthetic engine oil nanofluids have the potential to significantly advance the performance of solar parabolic collectors.

Keywords: Multi-walled carbon nanotube, Orthocresol, Solar parabolic collector, Sonication, Surfactant, Volume fractions

1 Introduction

In the face of rapid technological advancements and a pressing need for sustainable energy solutions, solar energy emerges as a key renewable resource to address the escalating global power demand. Solar energy can be harnessed through two primary technologies: 1) photovoltaic cells, which convert solar radiation directly into electricity but are limited by conversion efficiency. 2) Solar collectors, particularly parabolic collectors, are pivotal for a wide range of applications, from industrial processes to heating and power generation, due to their ability to concentrate solar radiation onto a focal line. The efficacy of these collectors can be further enhanced by employing nanofluids due to their superior heat transfer properties, promising significant improvements in thermal performance. The selection of solar collectors is contingent upon the application's specific temperature needs, and the integration of nanofluids has opened new avenues for optimizing the energy yield of parabolic collectors, as extensively reviewed in the literature.

Bellos *et al*., [1] advanced solar thermal technology by designing a parabolic collector tailored to concentrate solar radiation optimally within a temperature range of 150–400 °C. Their research employed numerical simulations to assess the performance of CuO nanoparticles suspended in Syltherm 800 and a molten nitrate salt mixture ($NaNO_3$:KNO_3 in a 3:2 ratio) as the working fluids. With a CuO nanoparticle volume concentration of 6%, they achieved operational temperatures of 377 °C for Syltherm 800 and 577 °C for the molten salt. The findings demonstrated a thermal efficiency improvement of 0.76% for the CuO-enhanced Syltherm 800 nanofluid and 0.26% for the CuO-enhanced molten salt, compared to their

respective base fluids, underscoring the potential of nanofluids in enhancing solar collector performance. Sokhansefat *et al*., [2] conducted a numerical study on Al_2O_3 nanoparticles in synthetic oil nanofluid within a solar parabolic collector at temperatures of 27 °C, 127 °C, and 227 °C. By varying Al_2O_3 volume fractions (0.01%, 0.03%, 0.05%), they examined the effect on thermal performance. The study highlighted a 3.8 °C absolute error between numerical and experimental temperatures, demonstrating model accuracy. Importantly, it revealed that increasing nanoparticle concentration enhances the convective heat transfer coefficient, suggesting improved solar collector efficiency.

Jamshed *et al*., [3] conducted a numerical analysis on the thermal efficiency of Cu-engine oil and Al_2O_3-engine oil nanofluids in a solar parabolic collector, with volume fractions of 0.03%, 0.05%, and 0.1%. The study found that the impact of these nanofluids on heat transfer was more significant near the tube wall and decreased towards the center. Furthermore, the Cu-engine oil nanofluid exhibited higher thermal efficiency compared to the Al_2O_3-engine oil nanofluid, highlighting its effectiveness in solar energy capture and conversion. Abubakr *et al*., [4] explored the impact of Al_2O_3, CuO, and SiO_2 nanoparticles in Therminol VP-1, Syltherm 800, and Dowtherm Q on the efficiency of solar parabolic trough collectors, under conditions of 1000 W/m^2 beam radiation, a 240.79 °C inlet temperature, and a Reynolds number of 2.915×10^5. Their analysis showed enhanced thermal efficiency with increased Reynolds numbers and nanoparticle concentrations, notably with CuO nanofluids showing superior performance. This study, in agreement with Bellos *et al*., highlights the critical role of base fluid choice in optimizing heat transfer, underscoring the importance of high heat-carrying capacities for improved efficiency.

Jamshed *et al*., [5] conducted a numerical assessment of Fe_3O_4-engine oil and Cu-engine oil nanofluids in a parabolic trough solar collector, exploring nanoparticle volume concentrations from 0.1% to 0.2% across different nanoparticle shapes: sphere, hexahedron, tetrahedron, column, and lamina. Their findings revealed that nanofluids with lamina-shaped nanoparticles exhibited superior performance due to their increased surface area interacting with the fluid. Additionally, Cu-engine oil nanofluids were found to have a more efficient heat transfer compared to Fe_3O_4-engine oil, highlighting the significance of nanoparticle composition and shape in enhancing the collector's thermal efficiency. Mwesigye *et al*., [6] performed numerical analyses of solar parabolic trough collectors with copper, silver, and aluminum oxide nanoparticles in Therminol oil, adjusting both the concentration ratio (from 88 to 113) and nanoparticle volume concentration (from 1% to 6%). Their study discovered optimal performance at a concentration ratio of 113, with silver nanoparticles in Therminol oil achieving the most significant thermal efficiency improvement of 13.9% over pure Therminol oil. This research highlights the pivotal role of nanoparticle type and concentration in maximizing solar collector efficiency. Bellos *et al*., [7] inspected the influence of the concentration ratio of a parabolic solar collector on its thermal efficiency. The results show that a higher concentration ratio intensifies the thermal performance of the collector, but the selection should depend on the required temperature and limitations of the application area. The analysis was further accomplished to improve thermal efficiency by modifying the absorbing tube with a sine geometrical shape to increase the surface area and effective turbulence for heat transfer, resulting in a 4.55% improvement. Utilizing Al_2O_3-thermal oil nanofluid as a working fluid enhanced the thermal efficiency by 4.25%, and pressurized water improved it by 6.34%.

Vahabzadeh *et al*., [8] explored the effectiveness of Al_2O_3 nanoparticles suspended in synthetic oil nanofluid within a parabolic trough collector featuring a porous receiver tube. The study varied parameters including the Reynolds number, nanoparticle volume fraction, inlet temperature, and Darcy number to assess their impact. Findings revealed that integrating porous media within the collector enhanced heat transfer efficiency, albeit at the cost of a higher pressure drop across the system. This investigation underscores the nuanced balance between improving thermal performance and managing fluid dynamics within solar collectors.

Liu *et al*., [9] investigated the enhancement of thermal conductivity in nanofluids containing multi-walled carbon nanotubes (MWCNT) dispersed in ethylene glycol and synthetic engine oil, with volume concentrations of 1% and 2%, respectively. Their findings indicated significant improvements in thermal

conductivity compared to the base fluids. Specifically, the thermal conductivity for the 1% ethylene glycol-based nanofluid saw an increase of 12.4%, while the 2% synthetic engine oil-based nanofluid exhibited a 30% increase. This research supports the potential application of MWCNT nanofluids in various industries due to their enhanced thermal properties. Guangul *et al*., [10] conducted a comprehensive study on various types of fuel cells, including Direct Methanol Fuel Cell (DMFC), Polymer Electrolyte Membrane Fuel Cell (PEMFC), Reversible Fuel Cell (RFC), Alkaline Fuel Cell (AFC), Phosphoric Acid Fuel Cell (PAFC), Molten Carbonate Fuel Cell (MCFC), and Solid Oxide Fuel Cell (SOFC). They delved into the operational characteristics, advantages, and limitations of each fuel cell type. The study concluded that the selection of a fuel cell should be based on the specific operational demands and working conditions of the intended application, highlighting the importance of matching fuel cell capabilities with application requirements.

Research articles [1]–[9] and Table 1 have made significant strides in solar thermal technology, showcasing the impact of nanofluids and innovative design on enhancing solar parabolic collector efficiency by using oil as base fluid. This work highlights the critical role of nanoparticle characteristics and the strategic selection of base fluids in improving heat transfer. Additionally, the exploration of fuel cell technologies [10] stresses tailoring energy solutions to specific operational needs, advocating an interdisciplinary approach to renewable energy advancements. Among all previous works, the effect of MWCNT-synthetic engine oil nanofluid is not employed in the solar parabolic collector. Building on these insights, this research explores the potential of MWCNT (Multi-Walled Carbon Nanotube) nanoparticles in synthetic engine oil to elevate solar parabolic collector performance. By examining various MWCNT concentrations and flow rates, this study aims to refine solar collector efficiency further, marking a pioneering effort to incorporate advanced nanomaterials in renewable energy systems, and broadening the scope for future innovations in solar energy applications.

Table 1: Recent research works on solar parabolic collector

Sl. No	Method	Base Fluid	Nanoparticle	Concentration (%)	Size (nm)	Flow condition	Remarks	Ref.
1	Numerical	Water	TiO_2	0.5, 1, 1.5 and 2%	40 nm	Turbulent flow Re 8000–24000	The absorber tube was designed with an oval rib and the highest heat transfer was achieved at Re 24000 with 2% concentration.	[11]
2	Experimental & numerical	Water	graphene (G)–Fe_3O_4	0.01, 0.05, 0.1 and 0.2%	G - 5 and 30 nm	2 L/min	Compared to the base fluid the hybrid nanofluid achieved an efficiency of 6.367%.	[12]
3	Experimental	Water	CuO	0.05, 0.075, and 0.1 mass %	10 nm	70 and 140 lit/h	An efficiency increase of 45.15%, 51.19% and 53.26% for 70 lit/h and 59.61%, 63.56% and 69.07% respectively for 140 lit/h mass flow rate	[13]
4	Experimental	Water	-	-	-	0.04, 0.05, 0.06, and 0.12 kg/s.	The finned spiral flow path receiver with a flow rate of 0.12 kg/s produced optimal performance among the selected water flow rates.	[14]
5	Experimental	Water	-	-	-	0.2–2 L/min	This study experimentally compared four novel shapes of cavity receivers: conical-cylindrical-conical (CCC) and double cylindrical, with conventional conical and cylindrical designs. Among the designs, CCC provides better heat transfer.	[15]

Table 1: (*Continued*) Recent research works on solar parabolic collector

Sl. No	Method	Base Fluid	Nanoparticle	Concentration (%)	Size (nm)	Flow condition	Remarks	Ref.
6	Numerical	Engine oil	Hybrid graphene and single-wall carbon nanotubes	Graphene 0–0.04 vol% and SWCNTs 0–0.4 vol%	-	Laminar flow	The results show that SWCNTs/ engine oil has a higher Nusselt number as compared to graphene/ engine oil.	[16]
7	Numerical	Synthetic oil	Cu	0.01, 0.03,0.05 vol%	< 100 nm	3000–6000 Reynolds number	Thermal and exergetic efficiency were improved by considering Copper nanoparticles in the base fluid.	[17]
8	Numerical	Syltherm oil	Al_2O_3	Up to 5%	-	Turbulent flow 4.5–8.5 kg/s	The design of the absorber tube is arranged by varying the number of flange-shaped turbulator from 10–20 the corresponding mass flow rate changed from 4.5–8.5 kg/s leading to a better convective heat transfer rate.	[18]
9	Numerical	Engine oil	Cu and Fe_3O_4	0.1, 0.15 and 0.18 vol%	-	Laminar flow	The thermal proficiency of Cu-EO and Fe_3O_4-EO were 1.6 and 14.9% better than engine oil.	[19]
10	Experimental	Water	Al_2O_3 and GO	0.2 wt%	30 nm	1, 3 and 5 L/min	The optimum increase in thermal efficiency was noted at a flow rate of 1 L/min, with approximately 63.2% improvement observed in GO nanofluid and 32.1% in Al_2O_3 nanofluid.	[20]

2 Materials and Methods

2.1 *Base fluid*

Synthetic engine oil is an excellent heat transfer fluid commonly used in engineering applications due to its superior properties. One of the most popular synthetic engine oils is the 5W30 Castrol synthetic engine oil. This oil was procured from Castrol authorized automobile shop, and composition of synthetic engine was confirmed through FTIR spectra results as shown in Figure 1, and Table 2 shows thermo-physical properties of 5W30 synthetic engine oil.

Table 2: Thermo-physical properties 5W30 synthetic engine oil (Source: Castrol product data sheet)

Properties	Method	5W30 Synthetic Engine oil
Density (15 °C)	ASTM D4052	850 kg/m^3
Kinematic viscosity (40 °C)	ASTM D445	58 × 10^{-6} m^2/s
Kinematic viscosity (100 °C)	ASTM D445	10 × 10^{-6} m^2/s
Flash Point	ASTM D93	201 °C

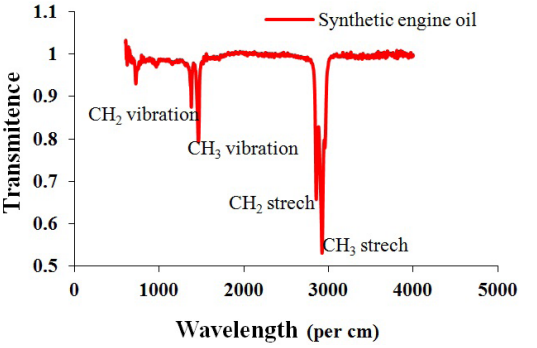

Figure 1: FTIR spectra of synthetic engine oil (Castrol).

2.2 *Nanoparticle*

The MWCNTs are the multiple cylindrical layers of the Graphene and it was procured by Adnano technologies private limited Shimoga, Karnataka, India. The MWCNT physical 2D structure is shown in Figure 2. The specifications of MWCNT are displayed in Table 3. The procured MWCNTs were harvested using the chemical vapor deposition method. The MWCNT was washed with de-ionized water

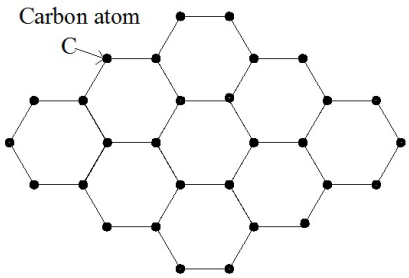

Figure 2: 2D structure of Multi-walled carbon nanotube (MWCNT).

and filtered. During the production or handling of MWCNTs, they may accumulate impurities such as residual catalyst particles, amorphous carbon, or other contaminants. Washing with de-ionized water helps to remove these impurities, ensuring a cleaner and more purified sample. Then the MWCNTs were dried at 80 °C for 2 h, as outlined by Aravind *et al*., [21]. Subsequently, the samples were subjected to TEM analysis to further examine their morphologies, including their shape, diameter, and any potential defects or impurities.

Table 3: Thermo-physical properties MWCNT [22]

Properties	MWCNT
Density (15 °C)	2100 kg/m^3
Thermal conductivity (35 °C)	2000 W/m K
Specific heat capacity (45 °C)	733 J/kg K

2.3 *Surfactant*

Surfactants are commonly used to stabilize nanoparticles in various fluids, including oils. In this context, the surfactant Orthocresol was used to stabilize MWCNTs (multi-walled carbon nanotubes) in synthetic oil. The chemical formula for Orthocresol is $(CH_3)C_6H_4OH$ or C_7H_8O. In the present work, the Orthocresol surfactant was procured by S D Fine-Chem. Ltd. Mumbai, Maharashtra, India and its chemical structure is shown in Figure 3.

2.4 *The equipments utilized in the formation of nanofluids and experiments of solar parabolic*

An electron microscope with exceptional high-resolution capabilities has been employed to examine the

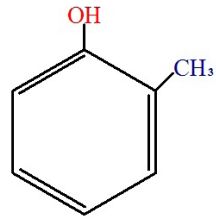

Figure 3: Orthocresol chemical structure.

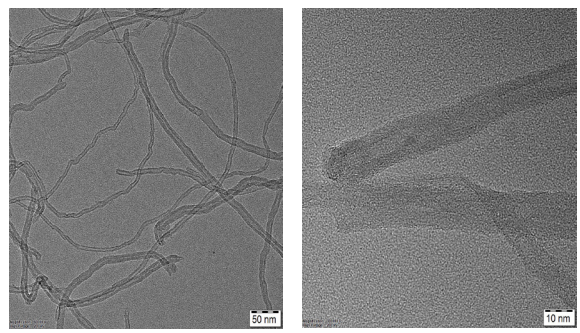

Figure 4: MWCNT TEM image.

MWCNT in order to confirm the physical structure and exhibited in Figure 4. TEM images confirmed the presence of multiple layers of nanotubes in the sample test. The magnetic stirrer is used to diffuse MWCNT in synthetic engine oil. The magnetic stirrer operating range was 0–1000 rpm and a standard variation of 10–20 rpm. The MWCNT nanofluid was further operated with an ultrasonic bath provided by Labman Scientific Instruments Private Limited and operating frequency of 40 ± 3 kHz.

During the experimental work on the solar parabolic collector, the solar radiation was measured by the pyranometer with an operating range of 0–2000 w/m^2 and a fluctuation of ± 5.5%. An anemometer was used to measure wind speed with a range of 0–45 m/s and ± 3% deviation, and the temperature of air was measured at 0–45 °C with a variation of ± 2 °C. The methodology to prepare nanofluids is shown in Figure 5.

2.5 *Methods employed to prepare nanofluids*

In this study, we used a two-step approach to prepare a carbon nanotube (CNT) nanofluid. The first step involved the preparation of a surfactant solution using Orthocresol dispersed in 5W30 synthetic engine oil. In the second step, multi-walled carbon nanotube

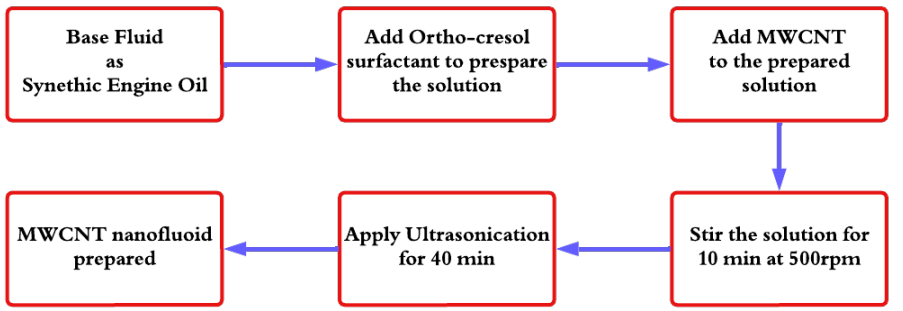

Figure 5: Steps involved in preparing the nanofluids.

(MWCNT) nanoparticles were added to the surfactant solution at a 1:1 ratio of Orthocresol to MWCNT, and the resulting solution was magnetically stirred for up to 10 min at 500 rpm. The solution was then ultrasonicated for 40 min to uniformly diffuse the MWCNTs in the solution [23], [24]. MWCNT volume concentrations of 0.0158, 0.0238, and 0.0317 vol% were considered to form the nanofluids. The stability of the MWCNT is explained in section 3.2.

2.6 *Thermo-physical properties of nanofluids*

To determine the volume fraction (ϕ) of MWCNTs added to the Synthetic engine oil depends on mass (m) and density (ρ) of base fluid (bf) and nanopartcles (np). It was estimated by Equation (1) [22], [25].

$$\phi = \left[\frac{\frac{m_{np}}{\rho_{np}}}{\frac{m_{np}}{\rho_{np}} + \frac{m_{bf}}{\rho_{bf}}} \right] \tag{1}$$

where m_{np} and m_{bf} are mass of the nanoparticle and base fluid in kg and ρ_{np} and ρ_{bf} are density of nanoparticles and base fluid respectively in kg/m^3.

The nanofluid density (ρ_{nf}) is a function of volume fraction (ϕ), density of nanoparticle ρ_{np} and base fluid density (ρ_{bf}) and it was evaluated by Pak & Xuan model Equation (2) [22], [25].

$$\rho_{nf} = \phi\rho_{np} + (1-\phi)\rho_{bf} \tag{2}$$

Where nanofluid density (ρ_{nf}) is measured in kg/m^3.

The nanofluid specific heat ($C_{p_{nf}}$) was dependent on volume fraction (ϕ), specific heat of nanoparticle ($C_{p_{np}}$) and specific heat of base fluid ($C_{p_{bf}}$). It was estimated through Equation (3) [22], [25].

$$C_{p_{nf}} = \phi C_{p_{np}} + (1-\phi)C_{p_{bf}} \tag{3}$$

where specific heat of nanofluid ($C_{p_{nf}}$) was measured in J/kg K.

The nanofluid thermal conductivity (k_{nf}) was calculated from Maxwell model Equation (4) [26].

$$k_{nf} = \frac{k_{bf}\left[2k_{bf} + k_{np} + 2\phi(k_{np} - k_{bf})\right]}{2k_{bf} + k_{np} - \phi(k_{np} - k_{bf})} \tag{4}$$

where k_{bf} and k_{np} are thermal conductivity of base fluid and nanoparticle, respectively. Thermal conductivity of nanofluid was measured in W/mK.

The nanofluid dynamic viscosity (μ_{nf}) was measured by using volume fraction (ϕ) and dynamic viscosity of base fluid (μ_{bf}) through Bachelor model Equation (5) [27].

$$\mu_{nf} = \mu_{bf}(1 + 2.5\phi + 6.5\phi^2) \tag{5}$$

where μ_{bf} is the dynamic viscosity of base fluid in Ns/m^2.

2.7 *The system configuration with the functioning of a solar parabolic collector*

Figure 6 illustrates the circuit flow of the working fluid, complete with flow control and temperature measurement instruments. Figure 7 depicts the solar parabolic collector's experimental setup, supplied by Ecosense in Delhi, India. Table 4 details the specifications of the experimental equipment. The study was conducted in Bengaluru, India (13°1'50" N –

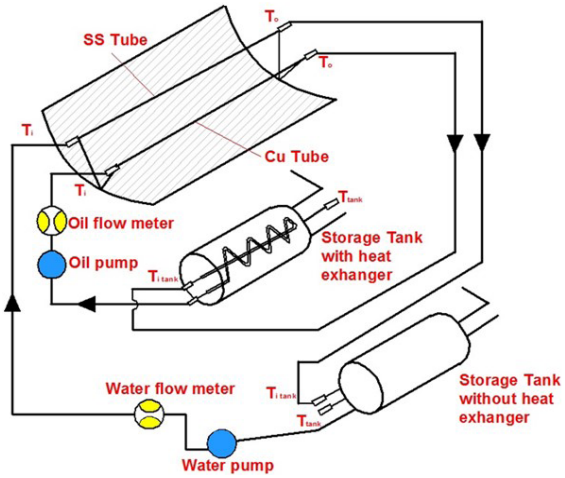

Figure 6: Schematic setup of solar parabolic collector.

77°33'54" E) and the solar collector was located in a north-south direction, with an auto-tracking mechanism that was adjusted every 20 min the position of a parabolic collector to the sun's traveling path. The experiments were carried out as per ASHRAE standard [28], taking into account different parameters such as incident radiation, ambient temperature, and consumption fluid temperature to estimate the overall thermal performance of the solar collector. The experimental data were collected at one-hour intervals from 10:00 to 16:00 for a single discharge, and the discharge was discrete at 6, 6.5, and 7 L/min.

Table 4: Specification of solar parabolic collector setup

Specification	
Parabolic trough mirror length	1.2192 m
Parabola aperture length	1.6764 m
Material of parabolic mirror	Acrylic
Focal position	0.6065 m
Rim Angle	67.24°
Internal diameter of receiver tube	0.023m
External diameter of receiver tube	0.025 m
Material of absorber tube	Copper tube

2.8 *Empirical relation used for thermal performance of solar parabolic collector*

The inlet and outlet temperatures of working media were varied at distinct time intervals, and the rate of heat absorption (q_u) was predicted using Equation (6) in watts [29].

Figure 7: Solar parabolic test rig.

$$\dot{q}_u = \dot{m} C_p (T_o - T_i) \tag{6}$$

where ($\dot{m}$) is the mass flow rate in kg/s, C_p is specific heat in J/kgK, T_o and T_i are temperature at outtlet and inlet of working fluid respectively in °C.

Equation (7) was employed to estimate the rate of heat absorption ($\dot{q}_u$), which is the change between the heat added and the heat lost through the absorber tube in watts [29].

$$\dot{q}_u = F_R (W - D_0) L \left\{ S - F_R U_l \frac{(T_i - T_a)}{S} \right\} \tag{7}$$

where F_R is heat removal factor, W is width of collector in m, D_o is outer diameter of absorber tube in m, L is length of absorber tube in m, S is radiation absorbed by tube in W/m^2, U_l is overall heat loss in W/m^{2}K, T_i is inlet temperature of working fluid in °C and T_a ambient temperature in °C. Equations (8) and (9) were considered to determine the instantaneous efficiency of solar parabolic collector (η_i) [29].

$$\eta_i = \frac{\dot{q}_u}{(A_c S)} = \frac{\dot{m} C_p}{A_c} \left[\frac{T_0 - T_i}{S} \right] \tag{8}$$

$$\eta_i = F_R \ (\tau\alpha) - (F_R U_l) \left[\frac{T_i - T_a}{S} \right] \tag{9}$$

where A_c is solar collector area in m^2 and $\tau\alpha$ is the transmitivity-absorbervity of absorber tube.

2.9 *Uncertainty analysis*

Standard uncertainty is an important factor for ensuring reliable and trustworthy results from the measurements. It is obtained from a combination of calibration data and manufacturer specifications, and taken into account device restrictions and inaccuracies in calibration. Standard uncertainty is typically measured as either standard deviation or increased uncertainty with a range element. This helps to assess the correctness and repeatability of measurements, which is crucial for more accurate evaluation and interpretation of results. The standard uncertainty of equipment was measured using Equation (10).

Standard uncertainty = (*Precision measurement value*)/√3 (10)

Equation (11) was considered to measure the uncertainty of the instantaneous efficiency ($\Delta\eta_i$) [30]–[32].

$$\Delta\eta_i = \left\{\left[\frac{\partial\eta}{\partial F_R}\Delta F_R\right]^2 + \left[\frac{\partial\eta}{\partial U_l}\Delta U_l\right]^2 + \left[\frac{\partial\eta}{\partial T_i}\Delta T_i\right]^2 + \left[\frac{\partial\eta}{\partial T_a}\Delta T_a\right]^2 + \left[\frac{\partial\eta}{\partial s}\Delta s\right]^2\right\}^{\frac{1}{2}} \quad (11)$$

Where ΔF_R change in heat removal factor, ΔU_l change in overall heat transfer coefficient, ΔT_i change in inlet temperature of working fluid, ΔT_a change in ambient temperature and Δs change in radiation absorbed by absorber tube. The overall uncertainty of the instantaneous efficiency ($\Delta\eta_i$) was estimated to be 5.5%. This value was obtained by taking into account the uncertainty of the discharges (±4.3%), and temperature sensors (±0.5 °C).

3 Results and Discussion

3.1 *5W30 synthetic engine oil as working fluid*

The experiments have been conducted during the period of 10:00 to 16:00 in January–February 2023.

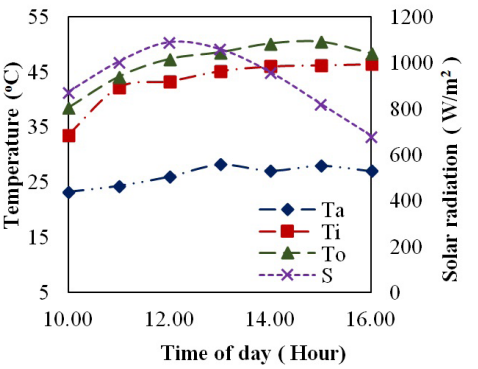

Figure 8: T_a, T_i, T_o and S trial data with respect to time of day at 6 L/min for synthetic engine oil.

Figure 8 represents the variation of intensity of solar radiation and temperature (ambient, fluid inlet & outlet) for synthetic engine oil as a working fluid with a discharge at 6 L/min. The intensity of solar emission and temperature has been noted at discharge of 6, 6.5 and 7 L/min.

The present experimental setup was conducted from 5–10 L/min for synthetic engine oil. But in the nanofluids, flow rate is suppressed up to 7 L/min. The reason is as the concentration of nanoparticles increases in the synthetic oil the viscosity of the fluid increases. Hence the chosen flow rates were determined through preliminary studies to maximize heat transfer efficiency within the system. Higher flow rates can enhance convective heat transfer, improving the overall efficiency of the solar collector. Due to this reason 6, 6.5 and 7 L/min discharge were conducted.

Figure 9 exhibits the instantaneous solar collector efficiency (η_i) versus the reduced temperature conditions, $T^* = \frac{(T_i - T_a)}{S}$ at different discharges. The data were formulated in the form of straight line equations and $F_R U_l$ and $F_R(\tau\alpha)$ results have been computed by affixing the data through linear equation for distinct discharges. The efficiency factors, $F_R U_l$ and $F_R(\tau\alpha)$ at every discharge are displayed in Table 5. A minimum result of $F_R U_l$ = 18.40 and a maximum value of $F_R(\tau\alpha)$ = 0.6329 were achieved at 7 L/min. $F_R(\tau\alpha)$ is pivotal in determining the collector's efficiency, as it quantifies the useful heat gain by the working fluid, which is directly tied to the mass flow rate of the working fluid through the collector, as outlined in Equation 9. An increase in mass flow rate enhances the interaction between the working fluid molecules

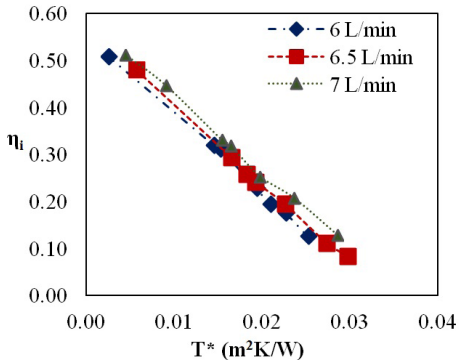

Figure 9: Instantaneous efficiency of a solar collector with respect to T^* at various discharges.

and the absorber tube, thereby augmenting useful heat gain. The observed range of $F_R(\tau\alpha)$ from 0.6061–0.6329 indicates a tangible improvement in collector efficiency with higher flow rates. This trend underscores the critical role of fluid dynamics in optimizing solar collector performance. These insights are valuable for designing more efficient solar thermal systems, as they highlight the importance of fluid properties and flow rates in achieving optimal heat transfer.

This also signifies a low flow resistance factor, leading to reduced pressure loss across the receiver tube and enhanced heat transmissivity within it. This amplifies the instantaneous efficiency of the solar collector. It was observed that the solar collector efficiency reached its maximum with an increase in discharge. This is attributed to the higher discharge, allowing more working fluid molecules to come into contact with the receiver tube, thereby facilitating increased heat interaction. Similar trend results were reported by Kumar *et al*., [11], Ram *et al*., [13] and Vishnu *et al*., [14].

Table 5: F_RU_l and $F_R(\tau\alpha)$ of solar parabolic collector at various synthetic engine oil discharges

Discharge (L/min)	F_RU_l	$F_R(\tau\alpha)$	R^2
6	19.87	0.6061	0.9961
6.5	19.47	0.6267	0.9977
7	18.40	0.6329	0.9972

3.2 *Intensity of surfactant over stability of multi-walled carbon nanotube nanofluids*

The nanofluids have been synthesized and excluded

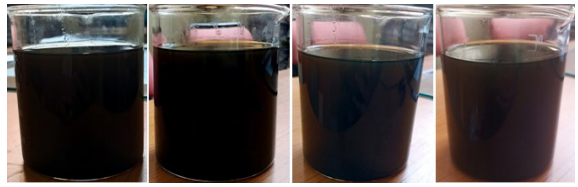

Figure 10: Stability of the MWCNT synthetic oil nanofluid.

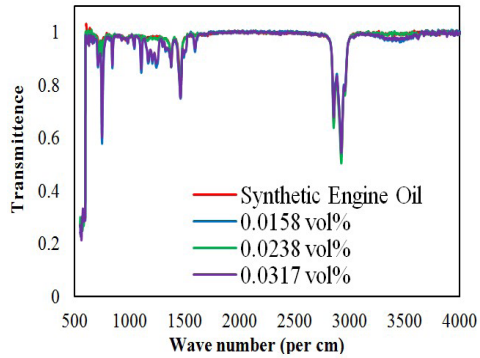

Figure 11: FTIR spectroscopy of synthetic oil nanofluid.

from the surfactant. The Multi-Walled Carbon Nanotubes (MWCNT) have been concentrated at the bottom of the vessel within a few minutes. This shows the instability of MWCNT nanoparticles. The reason is the MWCNT nanoparticles create strong Vander Waals forces. Hence, nanofluids were synthesized by introducing the effective intensity of the Orthocrisol surfactant. This results in an alteration of the exterior of the MWCNT. The influence of surfactant magnitude on the repulsive forces among the MWCNT particles prevented settling and remained stable. Figure 10 shows, the stability of MWCNT recorded by the photographic technique and maintained stability for a period exceeding 30 days [22]. Further, the transmittance spectra depicted in Figure 11 are crucial for understanding the interaction of light with the nanofluids. Each peak in the transmittance data correlates to the vibrational energies of the molecular bonds within the fluids. Variations in these spectra between the pure synthetic engine oil and the nanofluids indicate the addition of nanoparticles affects these molecular interactions. The stability of the nanofluid was inferred from the consistency of the spectra at different nanoparticle concentrations. The spectra remain similar across the concentrations, it implies that the nanoparticles

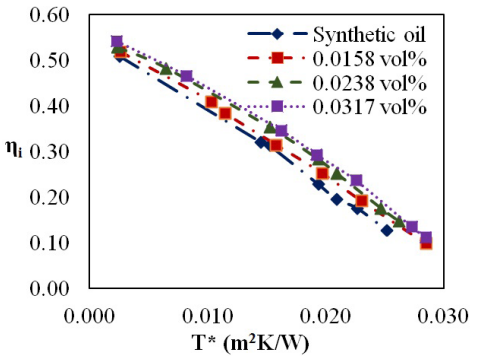

Figure 12: Instantaneous efficiency of collector η_i vs T^* at 6 L/min.

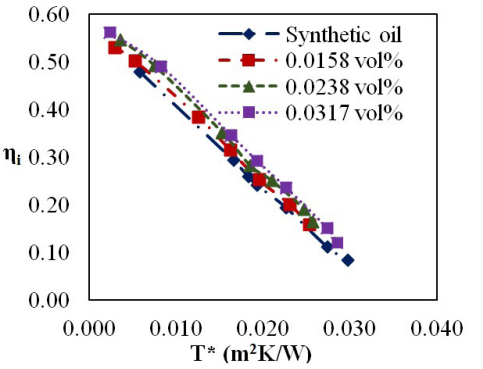

Figure 13: Instantaneous efficiency of collector η_i vs T^* at 6.5 L/min.

are evenly dispersed within the carrier fluid without significant agglomeration that would alter the molecular vibrations. This result confirms the even distribution of MWCNT nanoparticles in the synthetic engine oil [33]. Due to this the solar collector efficiency is enhanced through stable nanofluid.

3.3 *Intensity of distinct fractions of MWCNT nanoparticles in Synthetic engine oil*

The nanofluid was synthesized by volume fractions of 0.0158, 0.0238, and 0.0317% and Orthocrisol was blended with synthetic oil to advance stability. The intensity of different volume fractions on the instantaneous efficiency at various reduced temperatures $\frac{(T_i - T_a)}{S}$ at the discharge of 6, 6.5 and 7 L/min are displayed in Figures 12, 13 and 14. The solar collector was instantaneously boosted with incremental volume concentration for all discharges. For a discharge of 6 L/min with 0.0158 vol%, instantaneous efficiency improved by 1.06 % compared to synthetic engine oil. The efficiency increased by 2 and 3.3% at volume concentrations of 0.0238 and 0.0317%, respectively. Similar trends were observed for other discharges of 6.5 and 7 L/min. A maximum improvement of 6.95% in the efficiency was obtained with discharge 7 L/min and 0.0317 vol%. The volume fraction was increased by introducing nanoparticles into the base fluid, which increased the thermal conductivity. In this study, volume fractions of CNTs were maintained at lower values to attain optimal performance at the minimum price. Recent numerical analyses by Ghani *et al*., [16], Dou *et al*., [17], Shaker *et al*., [18], and Alkathiri *et al*., [19] have consistently demonstrated a trend similar to that observed in the current experimental work. This allows for optimal thermal management and efficient solar energy harvesting while avoiding the negative effects of high particle concentrations.

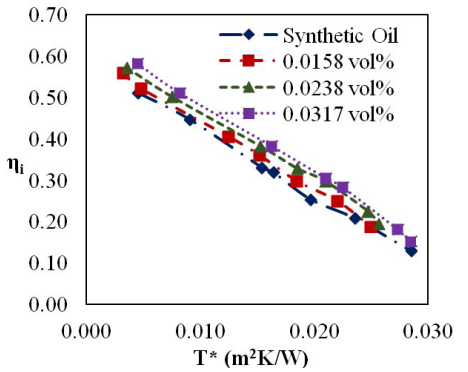

Figure 14: Instantaneous efficiency of collector η_i vs T^* at 7 L/min.

3.4 *The intensity of discharge on solar parabolic collector efficiency*

The results of the experiment showed that the instantaneous collector efficiency increased with an incremental nanofluid discharge. This is because, at a low discharge, the working fluid interacts with the receiver tube for a longer period, resulting in a higher temperature gradient and lower heat transfer. As the discharge of the working fluid increased, the temperature gradient decreased, resulting in an

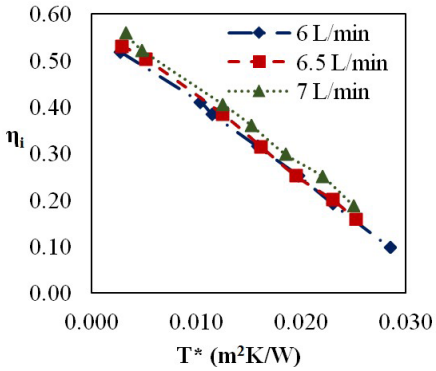

Figure 15: Instantaneous efficiency of collector η_i vs T^* at different discharge at 0.0158 vol%.

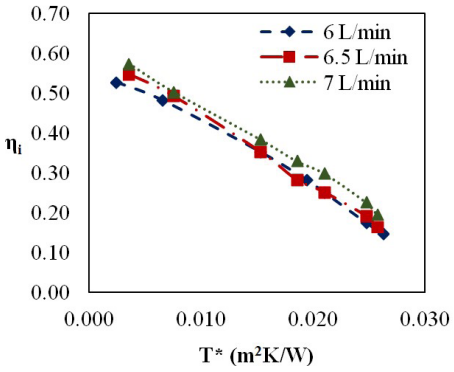

Figure 16: Instantaneous efficiency of collector η_i vs T^* at different discharge at 0.0238 vol%.

increase in the heat transfer coefficient and a diminution in the temperature difference between T_i and T_a. This results in a minimum estimate of T^* parameter ($T^* = \frac{(T_i - T_a)}{S}$), which in turn increases the solar collector efficiency. Figures 15, 16 and 17 show the effect of volume concentrations of 0.0158, 0.0238, and 0.0317 vol% with respect to the instantaneous collector efficiency at 6, 6.5 and 7 L/min successively. The results exhibited that the instantaneous collector efficiency increased with an increment in the volume concentration of the nanofluids, and that the effect was more pronounced at higher discharges. Overall, the experiment demonstrated that the employ of nanofluids could substantially improve the efficiency of instantaneous solar collectors, particularly at higher discharges and volume concentrations [34], [35].

The limitation of the present work in discharge depends on the pump capacity. For the particular

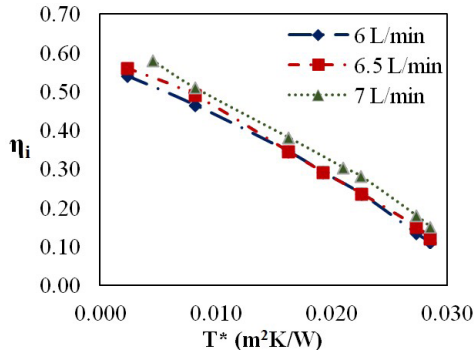

Figure 17: Instantaneous efficiency of collector η_i vs T^* at different discharge at 0.0317 vol%.

system, it is fixed hence we need to find the optimum discharge rate for all combinations of working fluid and choose the commending flow rates. As the volume concentration of nanoparticles increases in the base fluid, this leads to an increase in the viscosity of the working fluid and a large pressure drop. Moreover, beyond the optimal concentration, additional nanoparticle inclusion yields negligible heat transfer benefits due to decreased Brownian motion. Additionally, higher concentrations entail escalated operational expenses.

4 Conclusions

Conforming to ASHRAE standards, experimental investigations were conducted using a solar parabolic collector with nanofluids of varying volume fractions and at different discharge rates. The results revealed a notable correlation, with collector efficiency increasing alongside discharge increments. This relationship can be attributed to reduced temperature differentials between the working fluid and the receiver tube at higher discharges, facilitating a more efficient transfer of heat.

Introducing an optimal quantity of Orthocresol surfactant into the nanofluid played a pivotal role in enhancing the Brownian movement of MWCNT nanoparticles. This improvement resulted in heightened nanoparticle stability and, consequently, an enhancement in heat transfer efficiency. Furthermore, a progressive increase in the volume fraction of MWCNT nanoparticles in synthetic oil was identified as a means to enhance collector efficiency. However, this advancement also brought about an augmented resistance to fluid

flow, highlighting certain limitations in the effective incorporation of nanoparticles into the base fluid. In the ongoing investigation, remarkable collector efficiency was achieved at 7 L/min with a 0.0317 vol% nanofluid. Future work will extend these efforts by adopting various hybrid nanoparticles in synthetic engine oil and other working base fluids, aiming for continued advancements in performance.

Nomenclature

A_c	Area of the collector (m^2)
C	Concentration ratio
CNT	Carbon nanotube
C_p	Specific heat (J/kg K)
D	Diameter (m)
F_R	Collector heat removal factor
k	Thermal conductivity (W/mK)
L	Collector length (m)
L/h	Liter per hour
L/min	Liter per minutes
m	Mass (kg)
$\dot{m}$	Mass flow rate (kg/sec)
min	Minutes
MW	Mega watts
MWCNT	Multiwalled carbon nanotube
$\dot{q}_u$	Rate of heat gain (W)
Rpm	Revolution per minute
s	Global solar radiation (W/m^2)
T	Temperature (°C)
T^*	Reduced temperature ($K\text{-}m^2/W$)
TEM	Transmission Electron Microscopes
U_l	Overall coefficient loss (W/m^2K)
W	Collector width (m)

Greek symbols

ρ	Density (kg/m^3)
μ	Dynamic viscosity ($N\text{-}s/m^2$)
η_i	Instantaneous efficiency
T_a	Transmission-absorption factor
ϕ	Volume concentration (vol%)

Subscripts

a	Ambient
bf	Base fluid
i	Fluid inlet
nf	Nanofluid
np	Nano-particle
0	Fluid outlet

Acknowledgments

We extend our sincere thanks to M S Ramaiah institute of technology for providing experimental setup and conduct the experiments.

Author Contributions

V.T.: Investigation, Visualization, writing original draft; V.B.N.: Review and editing; G.L.: Conceptualization, investigation, visualization; P.B.N.: Review and editing the manuscript; All authors have read and agreed to the published version of the manuscript.

Conflicts of Interest

The authors declare no conflict of interest.

References

[1] E. Bellos, C. Tzivanidis, and D. Tsimpoukis, "Thermal, hydraulic and exergetic evaluation of a parabolic trough collector operating with thermal oil and molten salt based nanofluids," *Energy Conversion and Management*, vol. 156, pp. 388–402, 2018, doi: 10.1016/j.enconman.2017.11.051.

[2] T. Sokhansefat, A. B. Kasaeian, and F. Kowsary, "Heat transfer enhancement in parabolic trough collector tube using Al_2O_3/synthetic oil nanofluid," *Renewable and Sustainable Energy Reviews*, vol. 33, pp. 636–644, 2014, doi: 10.1016/j.rser.2014.02.028.

[3] W. Jamshed and K. S. Nisar, "Computational single-phase comparative study of a Williamson nanofluid in a parabolic trough solar collector via the Keller box method," *International Journal of Energy Research*, vol. 45, no. 7, pp. 10696–10718, 2021, doi: 10.1002/er.6554.

[4] M. Abubakr, H. Amein, B. M. Akoush, M. M. El-bakry, and M. A Hassan, "An intuitive framework for optimizing energetic and exergetic performances of parabolic trough solar collectors operating with nanofluids," *Renewable Energy*, vol. 157, pp. 130–149, 2020, doi: 10.1016/j.renene.2020.04.160.

[5] W. Jamshed, S. U. Devi S, R. Safdar, F. Redouane, K. S. Nisar, and M. R. Eid, "Comprehensive analysis on copper-iron (II, III)/oxide-engine oil Casson nanofluid flowing and thermal features in parabolic trough solar collector," *Journal of Taibah University for Science*, vol. 15, no. 1, pp. 619–636, 2021, doi: 10.1080/16583655.2021.1996114.

[6] A. Mwesigye and J. P. Meyer, "Optimal thermal and thermodynamic performance of a solar parabolic trough receiver with different nanofluids and at different concentration ratios," *Applied Energy*, vol. 193, pp. 393–413, 2017, doi: 10.1016/j.apenergy.2017.02.064.

[7] E. Bellos, C. Tzivanidis, K. A. Antonopoulos, and G. Gkinis, "Thermal enhancement of solar parabolic trough collectors by using nanofluids and converging-diverging absorber tube," *Renewable Energy*, vol. 94, pp. 213–222, 2016, doi: 10.1016/j.renene.2016.03.062.

[8] M. Vahabzadeh, M. Hossein, K. Hong, and Q. Xiong, "CFD study of heat transfer and fl uid fl ow in a parabolic trough solar receiver with internal annular porous structure and synthetic oil-Al_2O_3 nanofluid," *Renewable Energy*, vol. 145, pp. 2598–2614, 2020, doi: 10.1016/j.renene.2019.08.042.

[9] M. S. Liu, M. Ching-Cheng Lin, I. T. Huang, and C. C. Wang, "Enhancement of thermal conductivity with carbon nanotube for nanofluids," *International Communications in Heat and Mass Transfer*, vol. 32, no. 9, pp. 1202–1210, 2005, doi: 10.1016/j.icheatmasstransfer.2005.05.005.

[10] F. M. Guangul and G. T. Chala, "A comparative study between the seven types of fuel cells," *Applied Science and Engineering Progress*, vol. 13, no. 3, pp. 185–194, 2020, doi: 10.14416/j.asep.2020.04.007.

[11] A. Kumar, R. Kunwer, R. Kumar, and S. Kumar, "Case studies in thermal engineering effect of oval rib parameters on heat transfer enhancement of TiO_2/water nanofluid flow through parabolic trough collector," *Case Studies in Thermal Engineering*, vol. 55, Mar. 2024, Art. no. 104080, doi: 10.1016/j.csite.2024.104080.

[12] A. Y. Al-rabeeah, I. Seres, and I. Farkas, "Results in engineering experimental and numerical investigation of parabolic trough solar collector thermal efficiency enhanced by graphene – Fe_3O_4/water hybrid nanofluid," *Results in Engineering*, vol. 21, Mar. 2024, 2024, Art. no. 101887, doi: 10.1016/j.rineng.2024.101887.

[13] S. Ram, H. Ganesan, V. Saini, and A. Kumar, "Performance assessment of a parabolic trough solar collector using nanofluid and water based on direct absorption," *Renewable Energy*, vol. 214, pp. 11–22, 2023, doi: 10.1016/j.renene.2023.06.016.

[14] S. K. Vishnu and R. Senthil, "Experimental performance evaluation of a solar parabolic dish collector using spiral flow path receiver," *Applied Thermal Engineering*, vol. 231, 2023, Art. no. 120979, doi: 10.1016/j.applthermaleng.2023.120979.

[15] Q. Alkhalaf, D. Lee, R. Kumar, S. Thapa, A. R. Singh, M. N. Akhtar, M. Asif, and U. Ağbulut, "Experimental investigation of the thermal efficiency of a new cavity receiver design for concentrator solar technology," *Case Studies in Thermal Engineering*, vol. 53, 2024, Art. no. 103848, doi: 10.1016/j.csite.2023.103848.

[16] S. N. A. Ghani, R. Ul-Haq, and N. F. M. Noor, "Engine oil enhanced performance with hybrid graphene-SWCNT nanomaterials over a Riga curvy surface," *Case Studies in Thermal Engineering*, vol. 45, 2023, Art. no. 102902, doi: 10.1016/j.csite.2023.102902.

[17] L. Dou, B. Ding, Q. Zhang, G. Kou, and M. Mu, "Numerical investigation on the thermal performance of parabolic trough solar collector with synthetic oil / Cu nanofluids," *Applied Thermal Engineering*, vol. 227, 2023, Art. no. 120376, doi: 10.1016/j.applthermaleng.2023.120376.

[18] B. Shaker, M. Gholinia, M. Pourfallah, and D. D. Ganji, "CFD analysis of Al_2O_3 -syltherm oil Nanofluid on parabolic trough solar collector with a new flange-shaped turbulator model," *Theoretical and Applied Mechanics Letters*, vol. 12, no. 2, 2022, Art. no. 100323, doi: 10.1016/j.taml.2022.100323.

[19] A. A. Alkathiri, W. Jamshed, S. Uma, S. Devi, and M. R. Eid, "Galerkin finite element inspection of thermal distribution of renewable solar energy in presence of binary nanofluid in parabolic trough

solar collector," *Alexandria Engineering Journal*, vol. 61, no. 12, pp. 11063–11076, 2022, doi: 10.1016/j.aej.2022.04.036.

[20] S. M. S. Hosseini and M. S. Dehaj, "An experimental study on energetic performance evaluation of a parabolic trough solar collector operating with Al_2O_3/water and GO/water nanofluids," *Energy*, vol. 234, 2021, doi: 10.1016/j.energy.2021.121317.

[21] S. S. J. Aravind, P. Baskar, T. T. Baby, R. K. Sabareesh, S. Das, and S. Ramaprabhu, "Investigation of structural stability, dispersion, viscosity, and conductive heat transfer properties of functionalized carbon nanotube based nanofluids," *Journal of Physical Chemistry*, vol. 115, no. 34, pp. 16737–16744, 2011, doi: 10.1021/jp201672p.

[22] S. U. Ilyas, R. Pendyala, and M. Narahari, "Stability and thermal analysis of MWCNT-thermal oil-based nanofluids," *Colloids Surfaces A: Physicochemical and Engineering Aspects*, vol. 527, pp. 11–22, 2017, doi: 10.1016/j.colsurfa.2017.05.004.

[23] B. Sharma, S. K. Sharma, S. M. Gupta, and A. Kumar, "Modified two-step method to prepare long-term stable CNT nanofluids for heat transfer applications," *Arabian Journal for Science and Engineering*, vol. 43, no. 11, pp. 6155–6163, 2018, doi: 10.1007/s13369-018-3345-5.

[24] Babita, S. K. Sharma, and S. M. Gupta, "Synergic effect of SDBS and GA to prepare stable dispersion of CNT in water for industrial heat transfer applications," *Materials Research Express*, vol. 5, no. 5, 2018, doi: 10.1088/2053-1591/aac579.

[25] V. Talugeri, V. B. Nasi, and P. B. Nagaraj, "A review on the influence of carbon nanotube parameters in the base fluid to increase heat transfer in the solar collector," *International Journal of Ambient Energy*, vol. 43, no. 1, pp. 8613–8631, 2022, doi: 10.1080/01430750.2022.2102069.

[26] M. Shaker, E. Birgersson, and A. S. Mujumdar, "Extended Maxwell model for the thermal conductivity of nanofluids that accounts for nonlocal heat transfer," *International Journal of Thermal Sciences*, vol. 84, pp. 260–266, 2014, doi: 10.1016/j.ijthermalsci.2014.05.010.

[27] D. Korres, E. Bellos, and C. Tzivanidis, "Investigation of a nanofluid-based compound parabolic trough solar collector under laminar flow conditions," *Applied Thermal Engineering*, vol. 149, pp. 366–376, 2019, doi: 10.1016/j.applthermaleng.2018.12.077.

[28] H. P. Garg and J. Prakash, *Solari Energy - Fundamentals and Applications*. New Delhi, India: Tata McGraw-Hill, 2000, pp. 103–108.

[29] S. M. S. Hosseini and M. S. Dehaj, "An experimental study on energetic performance evaluation of a parabolic trough solar collector operating with Al_2O_3/water and GO/water nanofluids," *Energy*, vol. 234, 2021, doi: 10.1016/j.energy.2021.121317.

[30] J. Subramani, P. Sevvel, and S. A. Srinivasan, "Influence of CNT coating on the efficiency of solar parabolic trough collector using Al_2O_3 nanofluids - A multiple regression approach," *Materials Today: Proceedings*, vol. 45, no. 2, pp. 1857–1861, 2021, doi: 10.1016/j.matpr.2020.09.047.

[31] M. Alsaady, R. Fu, Y. Yan, Z. Liu, S. Wu, and R. Boukhanouf, "An experimental investigation on the effect of ferrofluids on the efficiency of novel parabolic trough solar collector under laminar flow conditions," *Heat Transfer Engineering*, vol. 40, no. 9–10, pp. 753–761, 2019, doi: 10.1080/01457632.2018.1442309.

[32] J. Subramani, P. K. Nagarajan, O. Mahian, and R. Sathyamurthy, "Efficiency and heat transfer improvements in a parabolic trough solar collector using TiO_2 nanofluids under turbulent flow regime," *Renewable Energy*, vol. 119, pp. 19–31, 2018, doi: 10.1016/j.renene.2017.11.079.

[33] L. Chen, H. Xie, Y. Li, and W. Yu, "Applications of cationic gemini surfactant in preparing multi-walled carbon nanotube contained nanofluids," *Colloids and Surfaces A : Physicochemical and Engineering Aspects*, vol. 330, pp. 176–179, 2008, doi: 10.1016/j.colsurfa.2008.07.047.

[34] M. Elmnefi, and W. Al-Khazraji, "Numerical and experimental studies of thermal performance enhancement for parabolic trough solar collector using none-circulated CuO/synthetic oil nanofluid," *International Journal of Numerical Methods for Heat & Fluid Flow*, vol. 33, no. 9, pp. 3124–3163, 2023, doi: 10.1108/HFF-11-

2022-0659.
[35] V. Talugeri, N. B. Pattana, V. B. Nasi, K. Shahapurkar, M. E. M. Soudagar, T. Ahamad, M. A. Kalam, K. M. Chidanandamurthy, N. M. Mubarak, and R. R. Karri, "Experimental investigation on a solar parabolic collector using water-based multi-walled carbon-nanotube with low volume concentrations," *Scientific Reports*, vol. 13, no. 1, pp. 1–11, 2023, doi: 10.1038/s41598-023-34529-6.